MXene-MOF architectural hybrid supported nickel single atom catalysts for hydrogen evolution reaction

Gayathri Chellasamy[a¶], Shiva Kumar Arumugasamy[b¶], Satheesh Kuppusamy[c], Viswanathan Ekambaram[d], Kandeeban Rajagopalan[e], Sada Venkateswaralu[f], Prabhakaran Deivasigamani[c], Min Jae Choi[b], Saravanan Govindaraju[a]*, Kyusik Yun[a]*

[a] Department of Bionanotechnology, Gachon University, Gyeonggi-do, 13120, Republic of Korea.

[b] Department of Chemical and Biochemical Engineering, Dongguk University, Seoul, 04620, Republic of Korea.

[c] Department of Chemistry, School of Advanced Sciences, Vellore Institute of Technology (VIT), Vellore, Tamil Nadu 632014, India.

[d] Department of Physics, Sri Sairam Institute of Technology, Chennai, Tamil Nadu, India

[e] Department of Chemistry, Kongunadu Arts and Science College, Coimbatore, Tamil Nadu, India

[f] Department of Chemistry, Gachon University, Gyeonggi-do, 13120, Republic of Korea.

AUTHOR INFORMATION

Corresponding Authors

*E-mail: biovijaysaran@gmail.com (S.G), ykyusik@gachon.ac.kr (K. Yun)

¶ Equal contribution

Chemicals

MAX phase of high purity (200 Mesh) was purchased from Heepani Tools store, China. Iron (III) chloride hexahydrate, 2-aminoterepthalic acid, nickel (II) nitrate hexahydrate, hydrofluoric acid, dimethyl sulfoxide, were purchased from Sigma-Aldrich, Republic of Korea. All the chemicals were of high purity and was utilized without any further refinement.

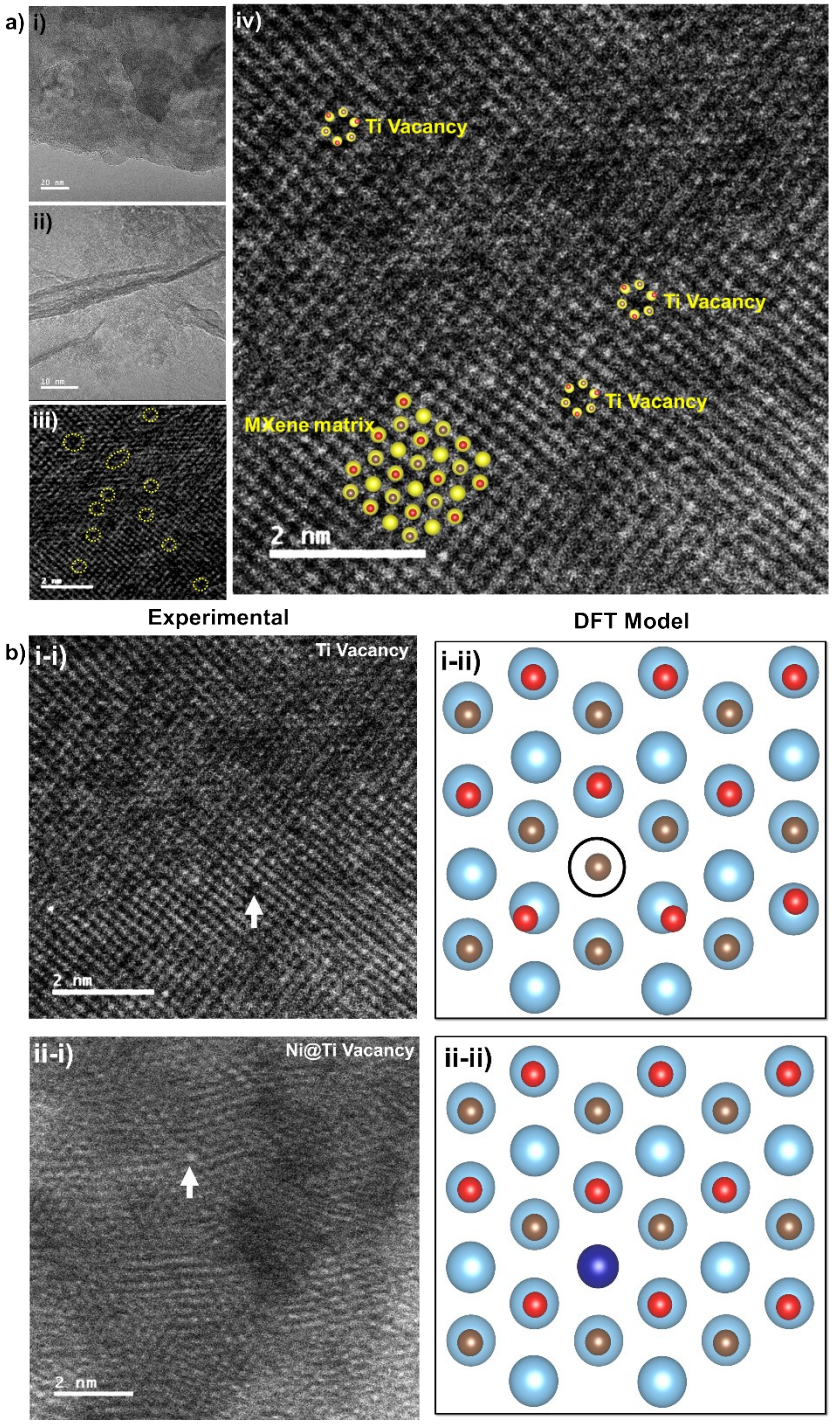

Supplementary figures

Fig S1. a) Vacancy site analysis of MXene i, ii) TEM images of MXene iii) HAADF-CS-STEM image of Ti vacancies on MXene surface (yellow colored circles denotes the vacancies) iv) HAADF-CS-STEM image of Ti vacancies on MXene surface (inset: simulated DFT model of Ti vacancy site and regular MXene matrix) **b)** i-i, i-ii) Comparison between experimental HAADF-STEM image, defect crystal structure determined from DFT of Ti vacancy MXene (Vc MXene) (inset: white arrow and black circle denote the Ti vacancy at MXene) ii-i, ii-ii)

Comparison between experimental HAADF-STEM image, Ni occupied defect crystal structure determined from DFT of Ni@Vc MXene) (inset: white arrow and blue sphere denote the Ni occupied at Vc MXene)

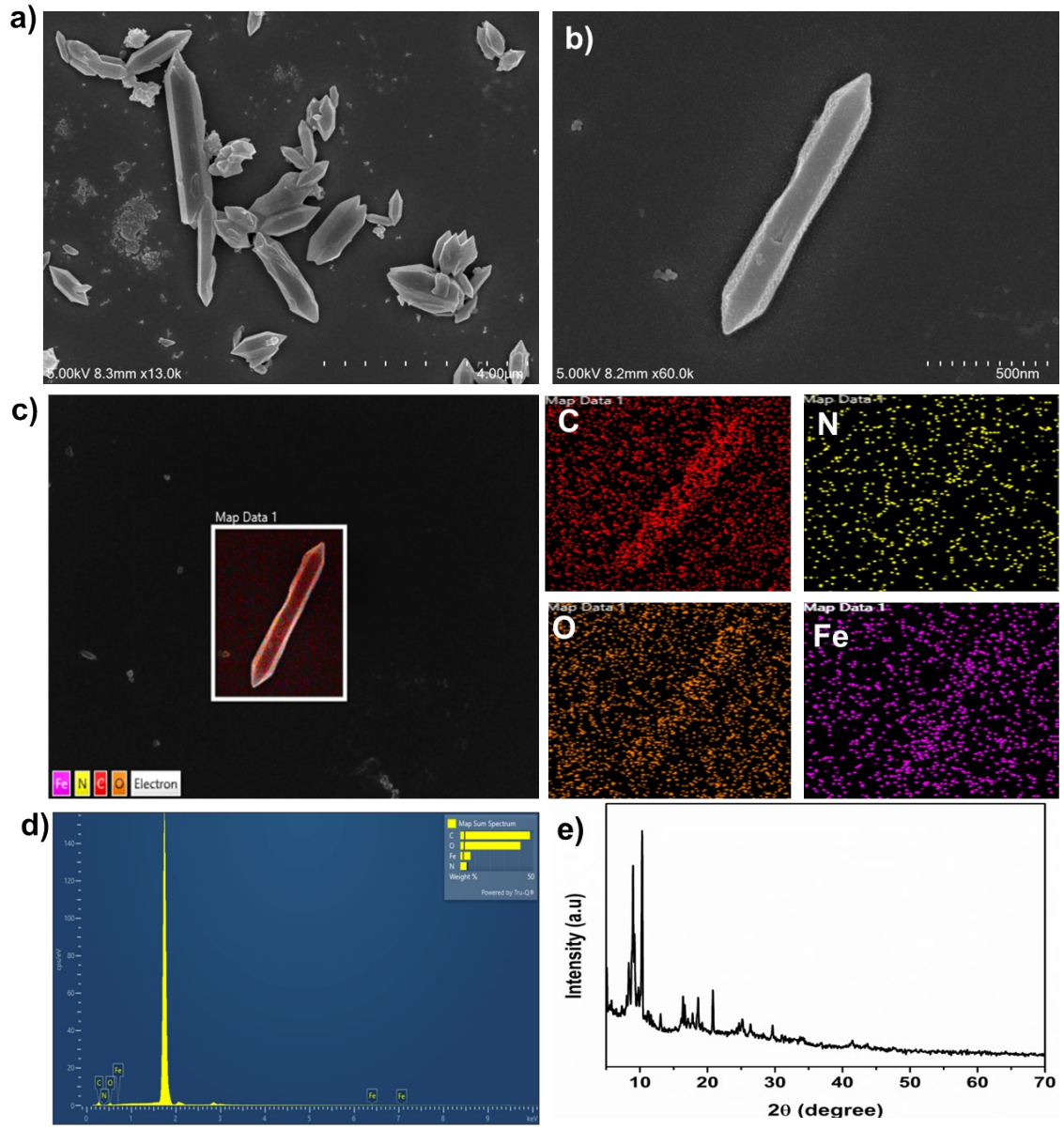

Fig S2. a, b) SEM images of Fe MOF under different magnification **c, d)** EDS mapping images of Fe-MOF **e)** XRD pattern of as-synthesized Fe-MOF

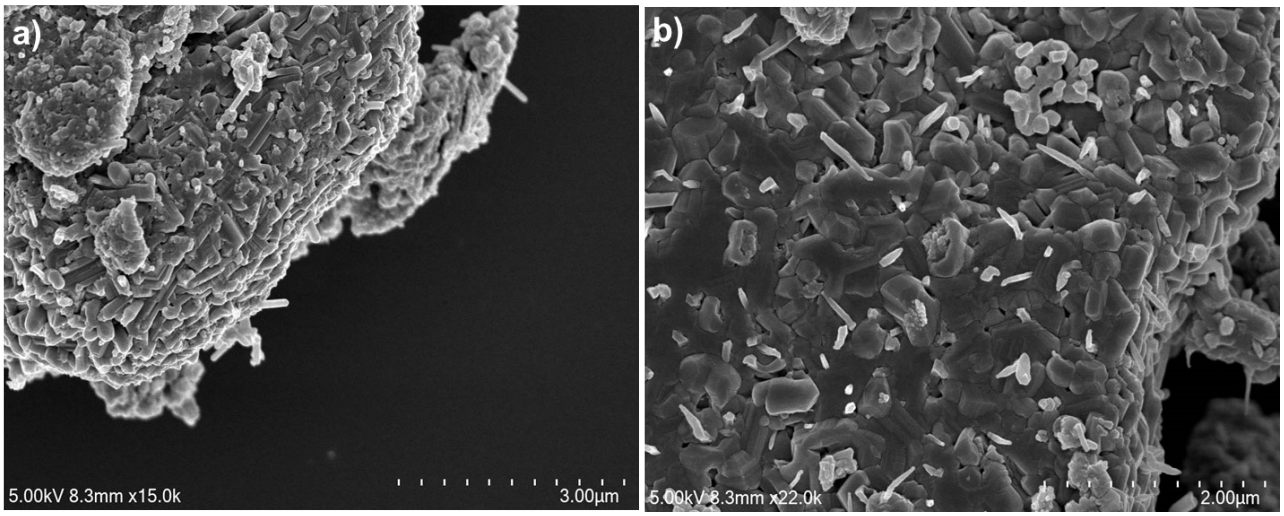

Fig S3. a, b) SEM images of MFN catalysts before thermal decomposition at different magnification

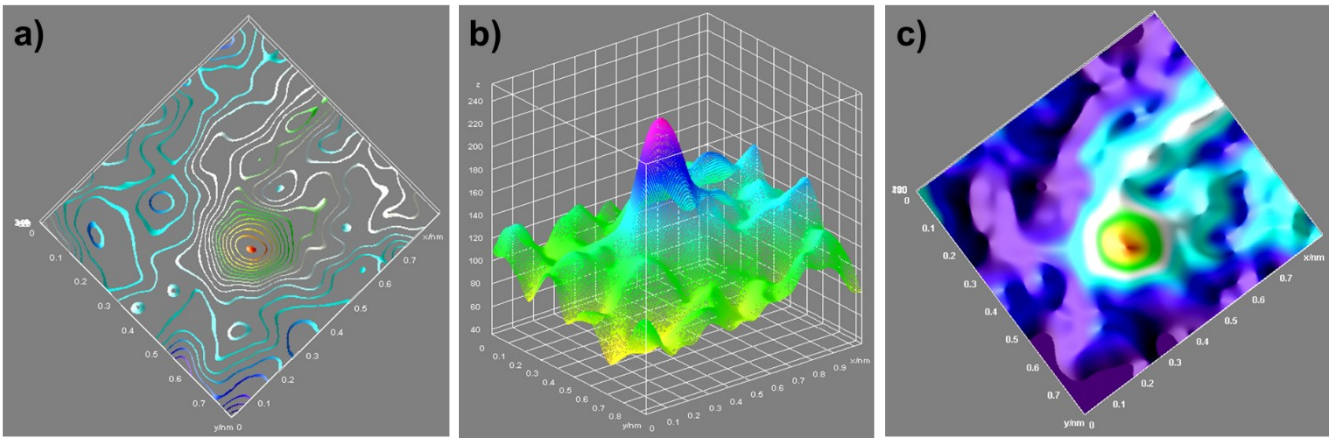

Fig S4. a) 3D isolines **b)** 3D atom overlapping **c)** Gaussian-function fitting mapping of Ni SACs of MFN catalyst from Figure 2b.

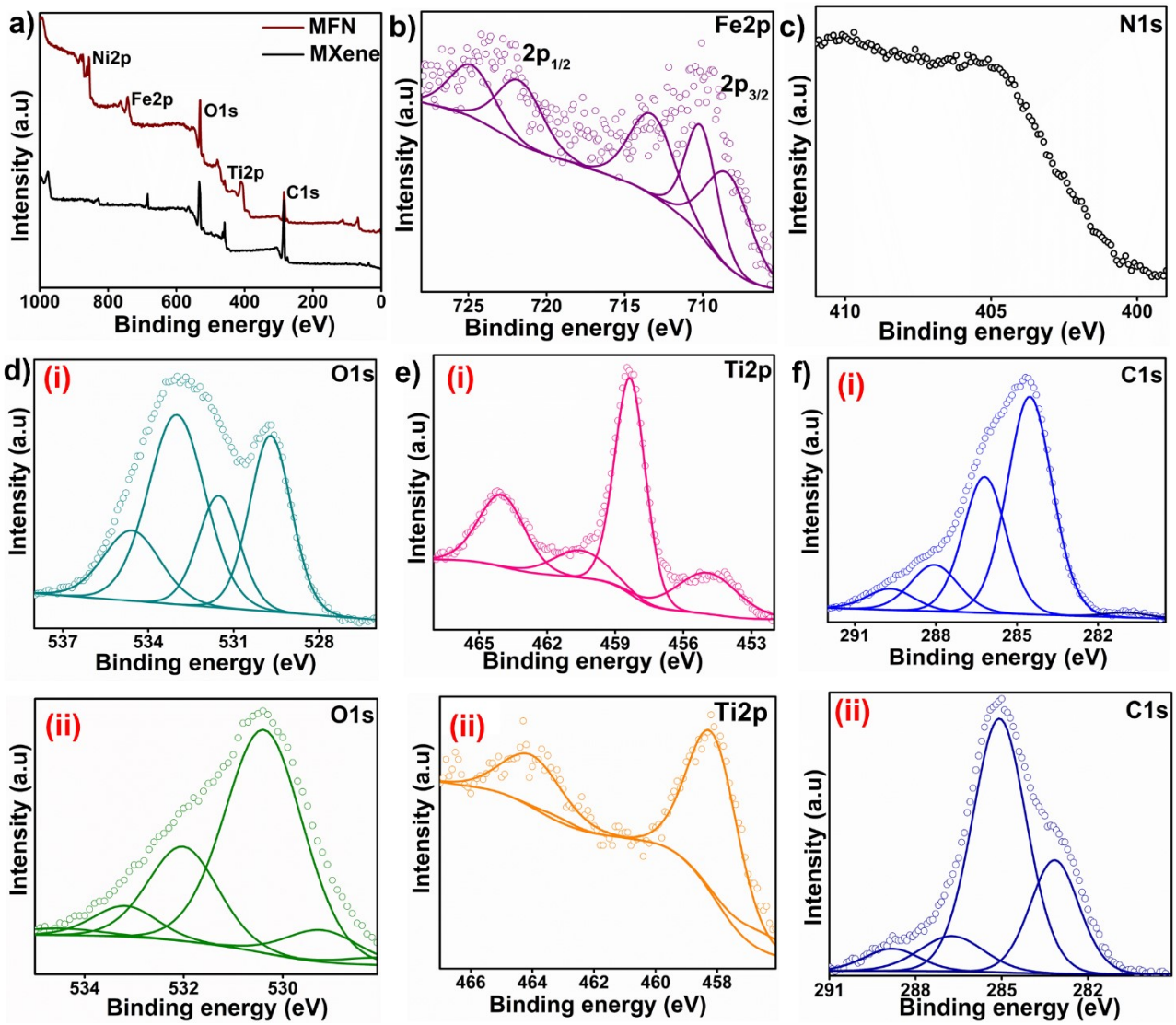

Fig S5. a) Overall survey spectra of MXene and MFN catalyst **b)** Deconvoluted Fe2p spectra of MFN **c)** N1s spectra of MFN **d-f)** (i) Deconvoluted O1s, Ti2p, C1s spectra of MXene (ii) Deconvoluted O1s, Ti2p, C1s spectra of MFN

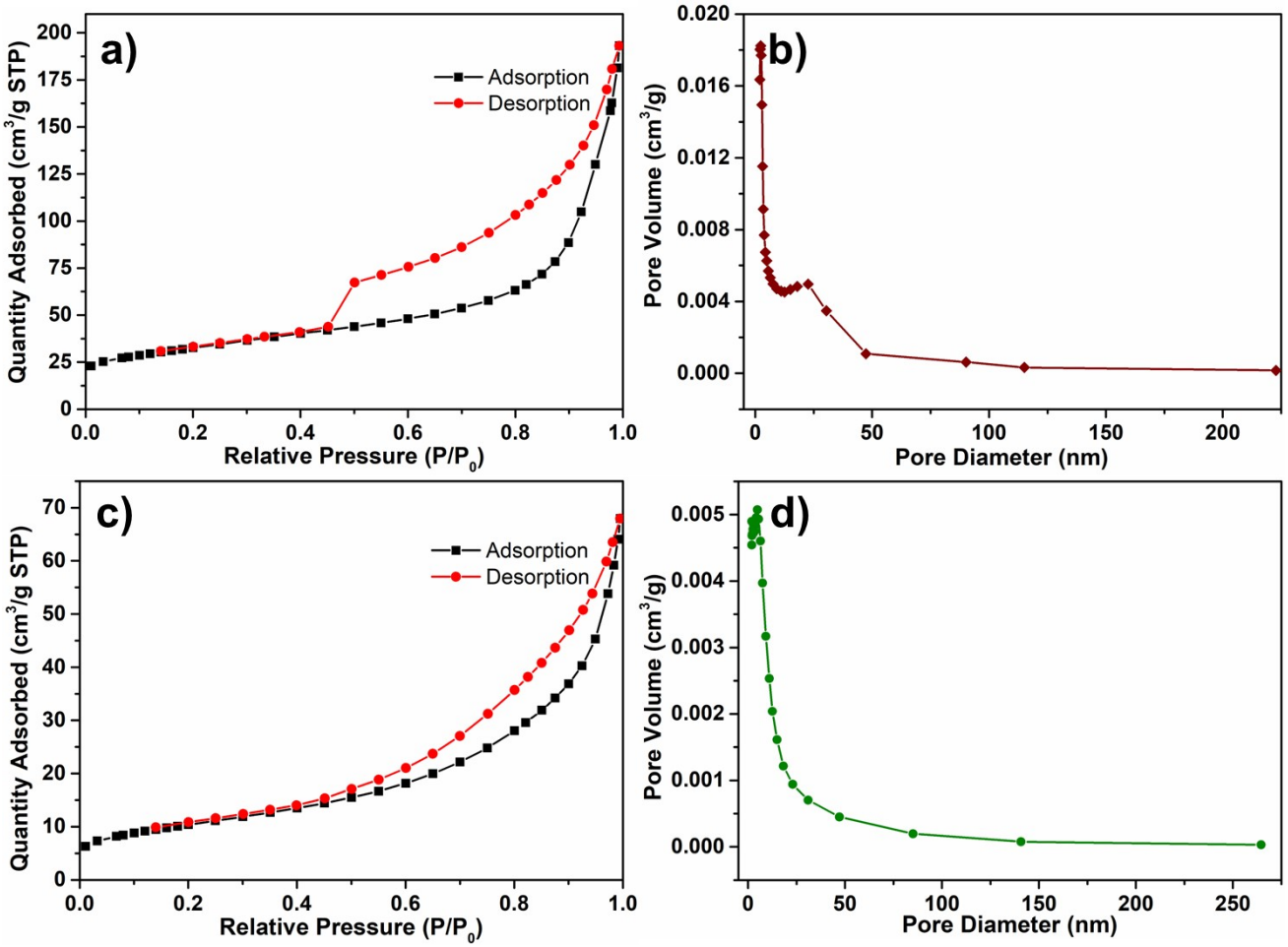

Fig S6. N_2 adsorption-desorption isotherms and pore size distribution estimated by NLDFT method for of **a, b)** MXene **c, d)** MFN catalyst

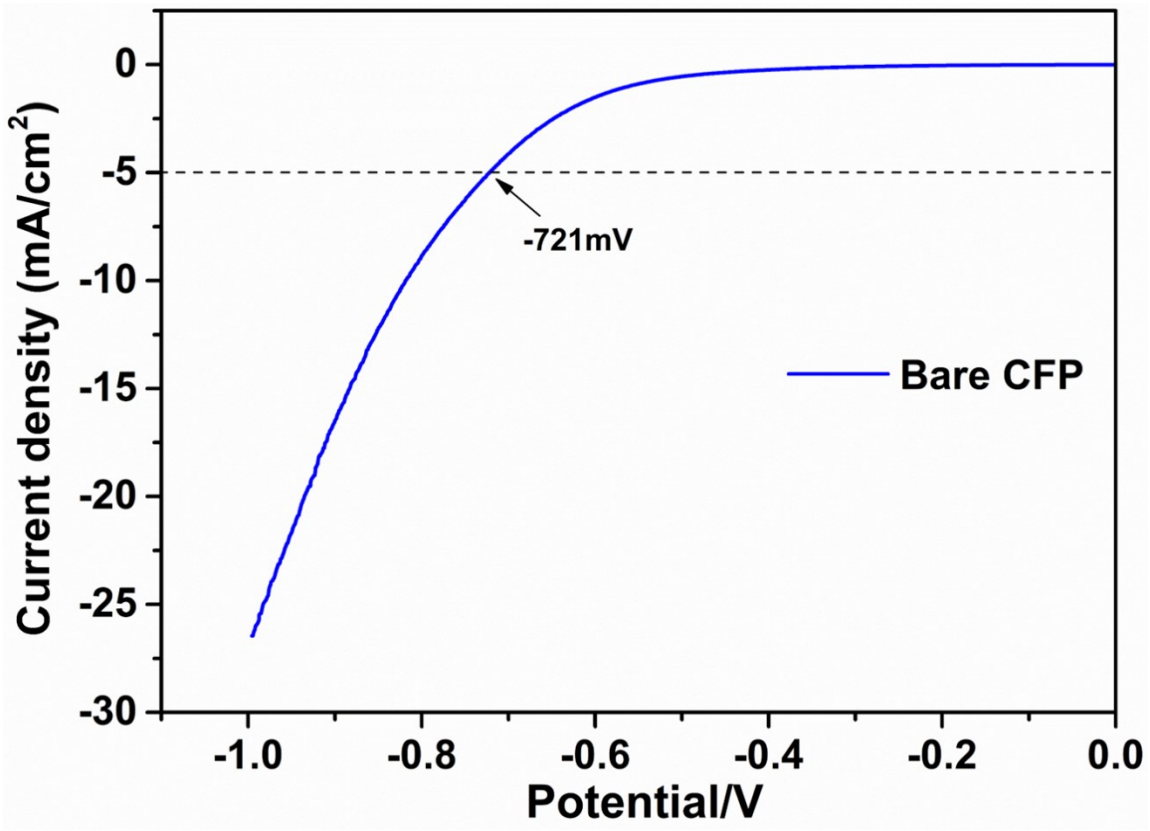

Fig S7. LSV polarization curve for the bare carbon fiber paper (CFP)

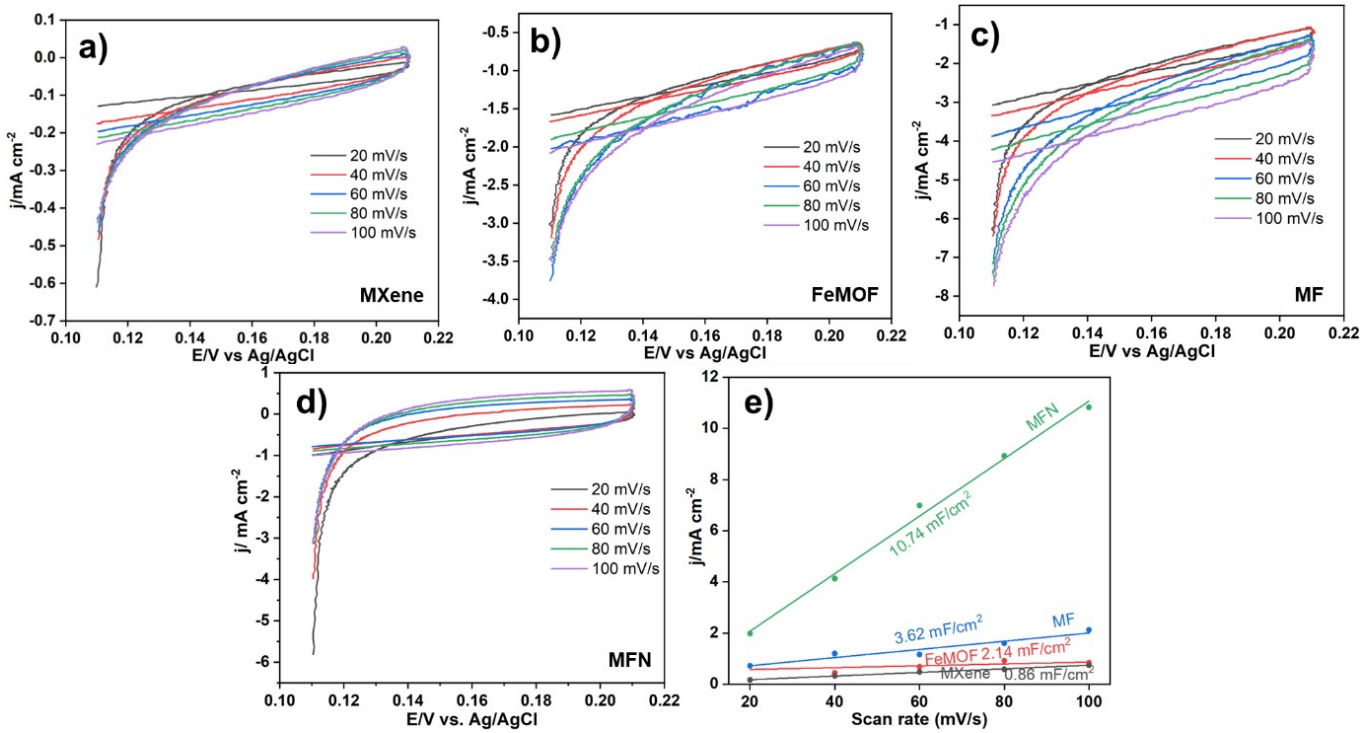

Fig S8. a-d) CV regimes in the potential window of 0.1-0.2 V in the non-faradic region to assess the double layer capacitance **e)** Plot illustrating the C_{dl} values of the developed catalysts

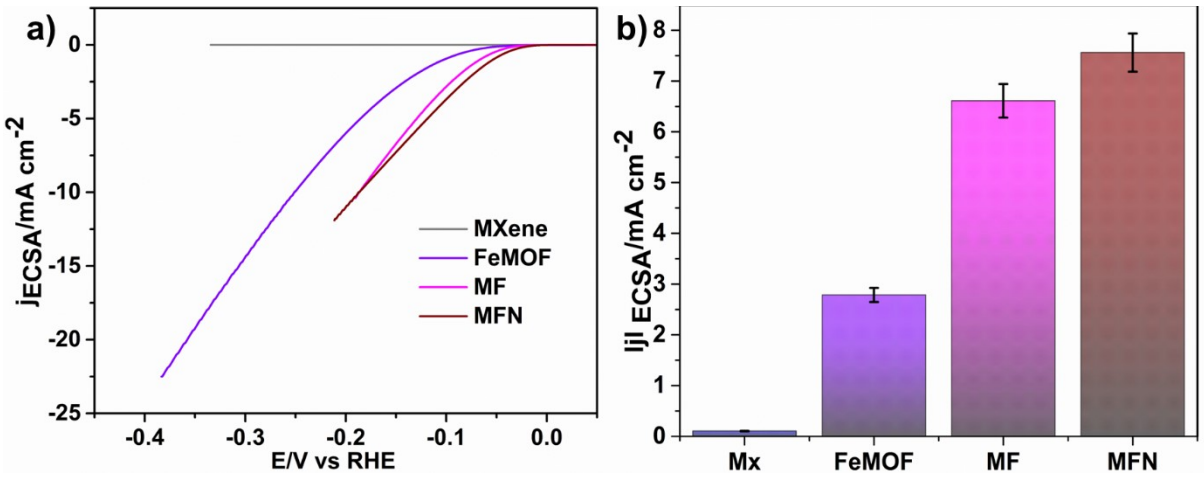

Fig S9. a) LSV polarization curves estimated from the ECSA values b) corresponding bar diagram elaborating the variation in current density at a constant 0.15V vs RHE

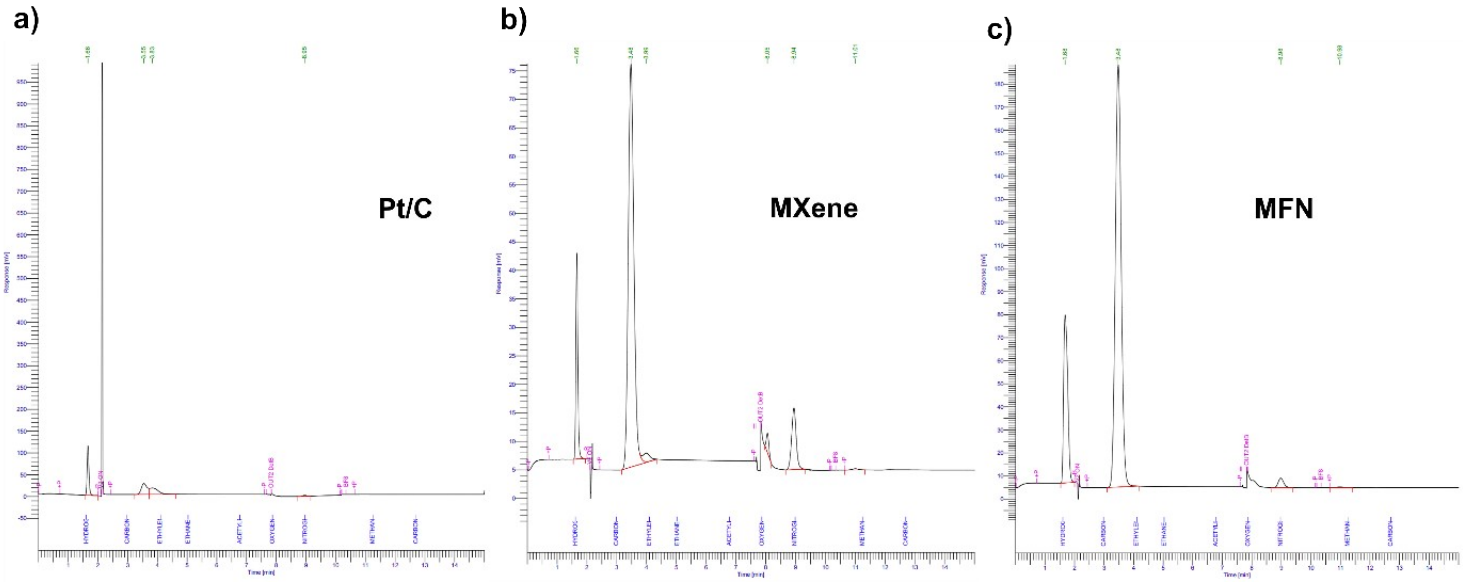

Fig S10. Representative GC chromatogram for **a)** Pt/C, **b)** MXene **c)** MFN catalyst after bulk electrolysis process

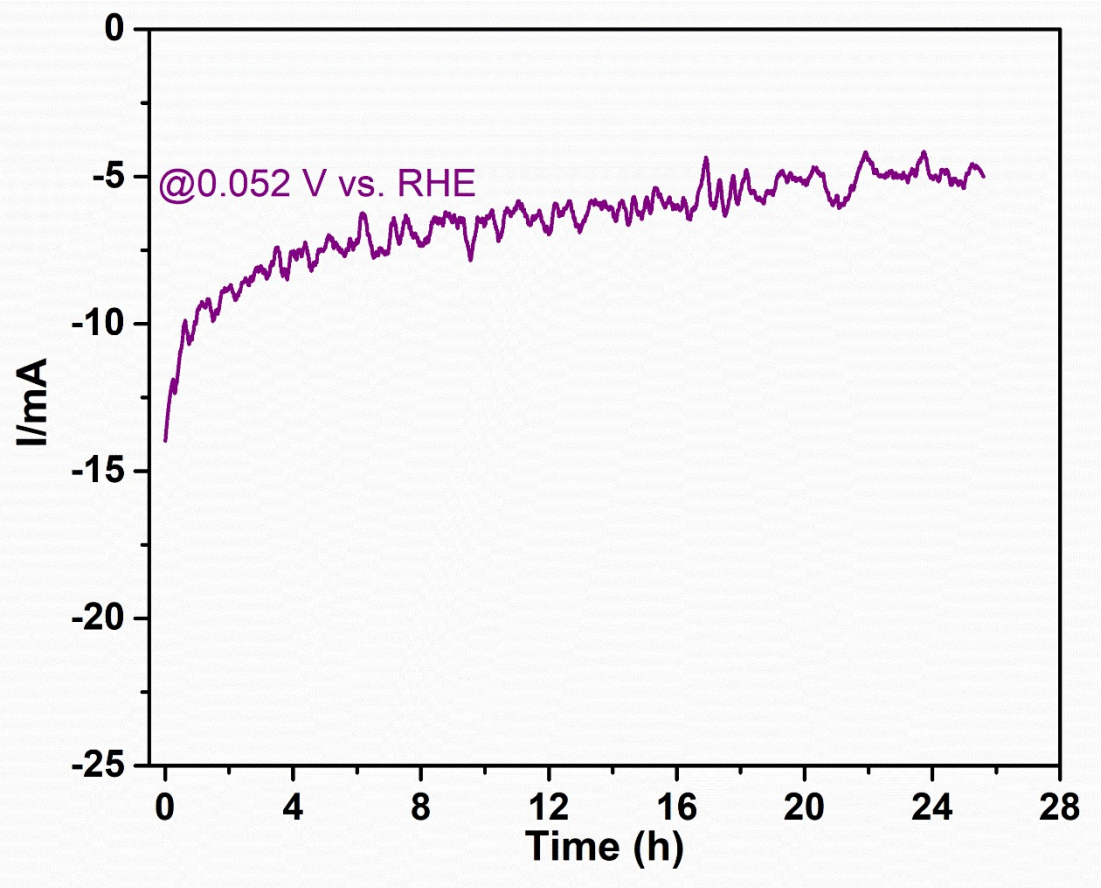

Fig S11. Chronoamperometry study for the MFN catalyst for assessing the stability of the material

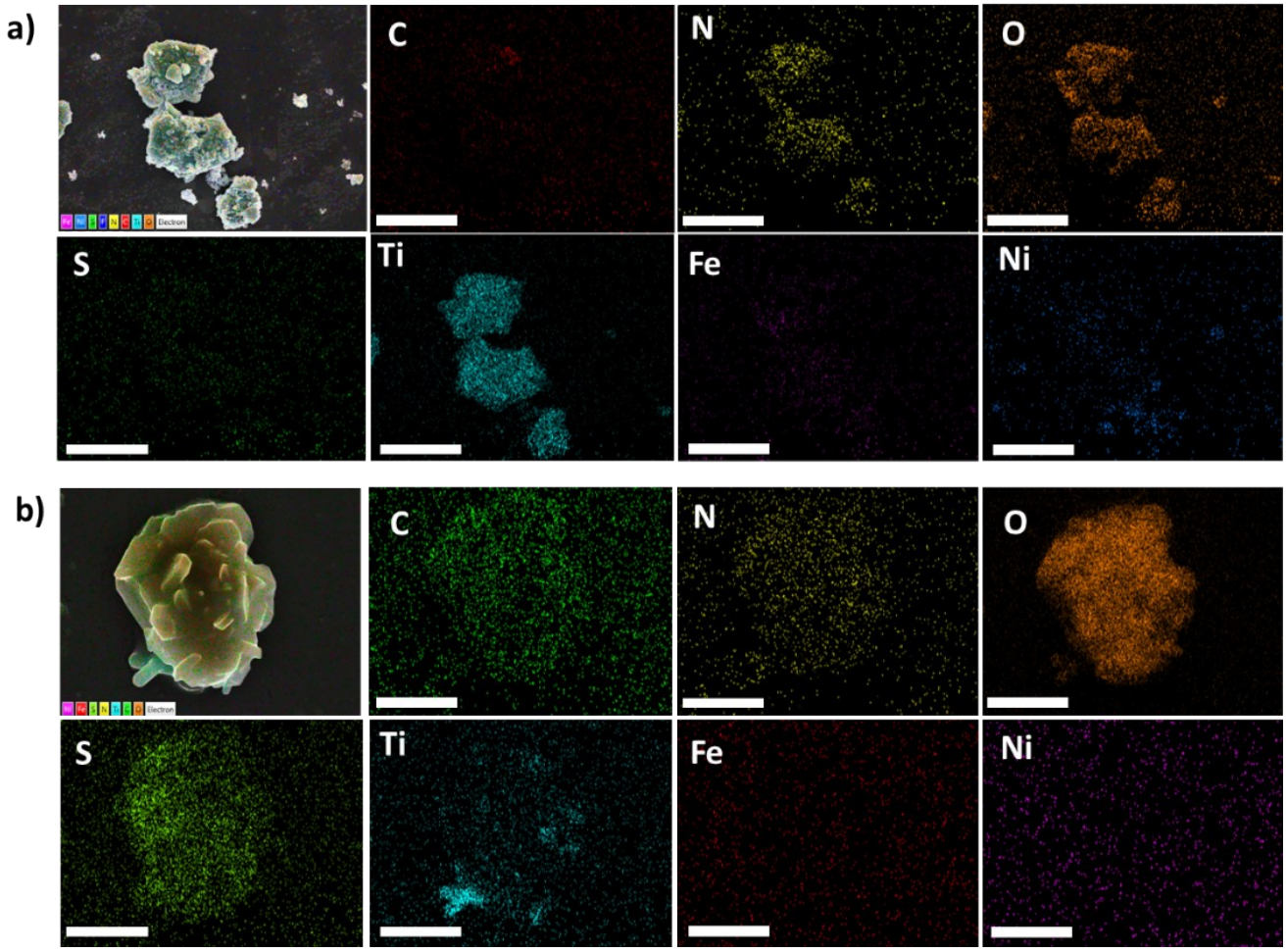

Fig S12. a, b) EDS mappings of post catalytic MFN observed at two different sites [scale bar a) 10µm and b) 2.5µm].

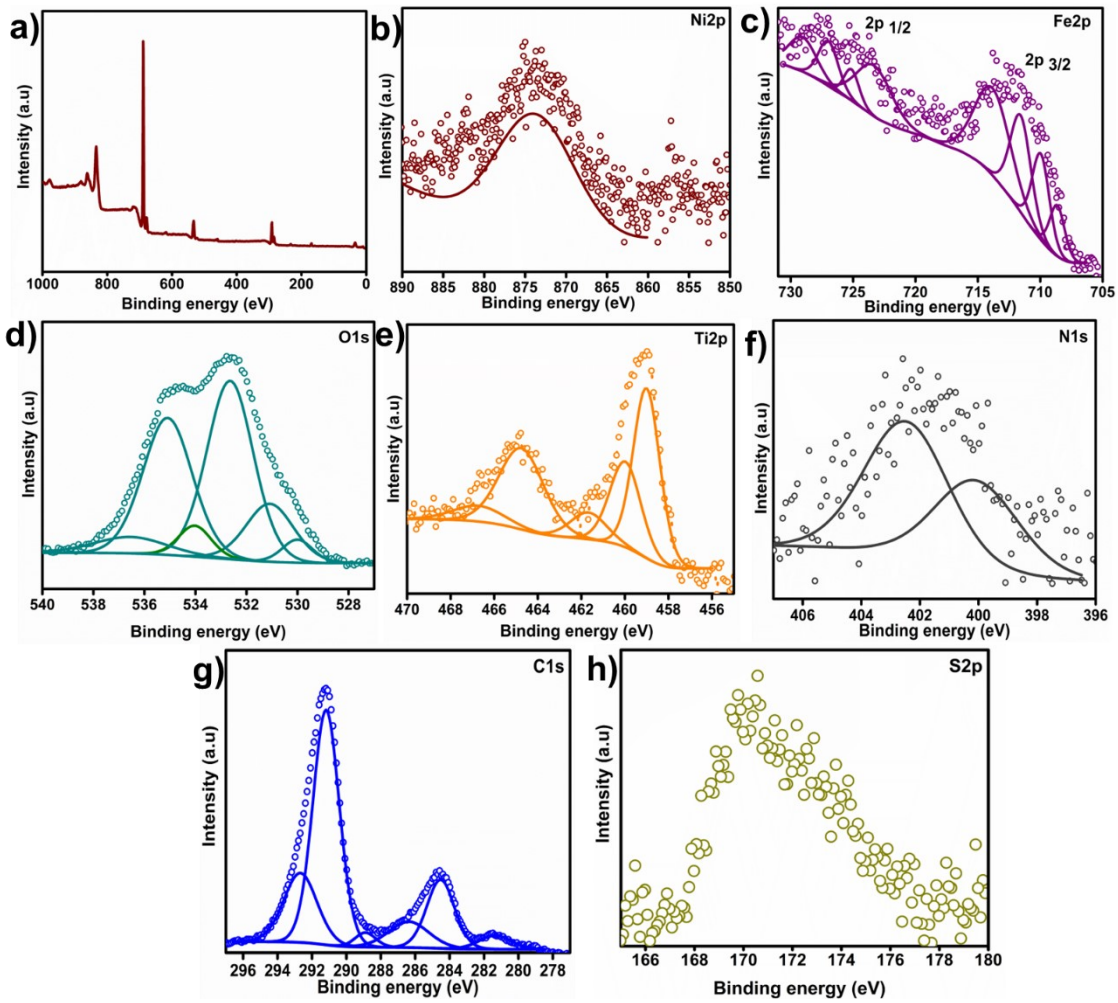

Fig S13. a) Overall survey spectra of post-catalytic MFN **b-g)** Deconvoluted Ni2p, Fe2p, O1s, Ti2p, N1s, C1s spectra of post-catalytic MFN

Supplementary discussion

XPS analysis was carried out to examine the chemical composition and surface electronic structure of thermal decomposed Fe-MOF before and after catalytic activity. The carbon peaks at 284.7 eV, 285.2 eV, and 288.8 eV are ascribed to the carboxylate (O–C=O) group in, the C–O link, and the C=C bond of the benzoic ring. The O1s spectra correspond to the 531.2 eV, 531.5 eV, 531.9 eV, and 532.5 eV, which are attributed to the lattice hydroxyl groups, the linkers C–O and O–C =O, and the adsorbed molecular water[1]. The N 1s spectrum, which is attributable to the N molecules in the amine group linker, has a peak at 398.96 eV[2] (Fig S14 a-d). Due to the valence, the interaction of outgoing electrons, surface oxidation, and the adsorption of water molecules during the catalytic activity, elements like C, N, and O gained prominent satellite peaks after the catalytic reaction and shifted towards the high binding energy in post-catalytic Fe-MOF[3]. Additionally, S2p found in Fe-MOF post-catalytic performance, the high-resolution S2p spectrum reveals peaks that correspond to the catalytic reaction in sulfuric acid, which helps to convert metal compounds to metal hydroxides and enhance the catalytic reaction. These peaks correspond to SOxn− at 161.70 eV, C–S–C at 162.67 eV and 163.97 eV, and Co–S bonds at 165.32 eV and 168.63 eV. The electrochemical reaction's proton electrosorption and surface adsorbed hydrogen recombination are represented by the conversion of H+ to H2 toward the HER reaction in the acidic medium[4] (Fig S14 e-i). For further confirmation, we have performed the SEM elemental mapping for the after catalytic sample of pyrolyzed Fe-MOF. Fig 15a, b shows the presence of elements C, N, Fe, O, with added element S presenting the participation of Fe-MOF in catalytic reaction.

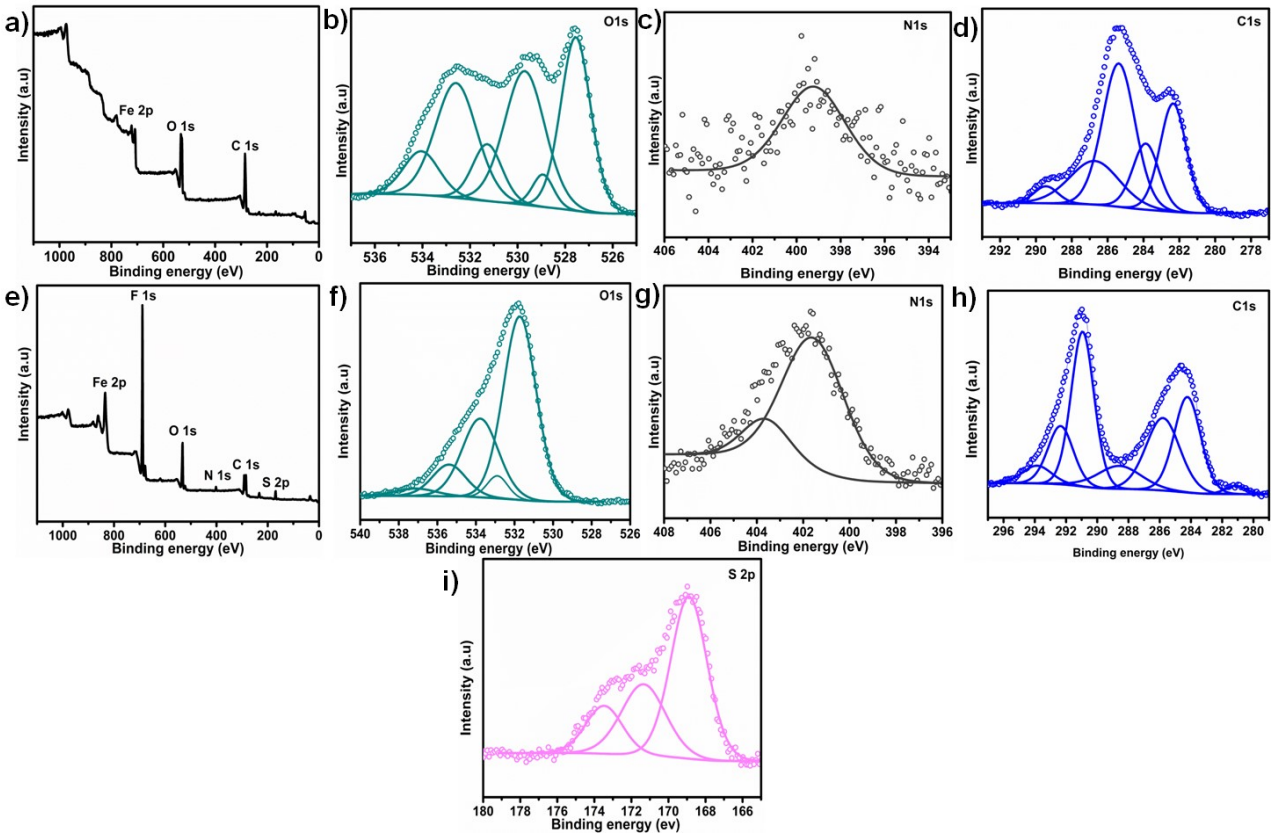

Fig S14. a) Overall survey spectra and **b-d)** Deconvoluted O1s, N1s, C1s spectra of pre-catalytic thermal decomposed Fe-MOF **e)** Overall survey spectra and **f-i)** Deconvoluted O1s, N1s, C1s, S2p spectra of post-catalytic thermal decomposed Fe-MOF

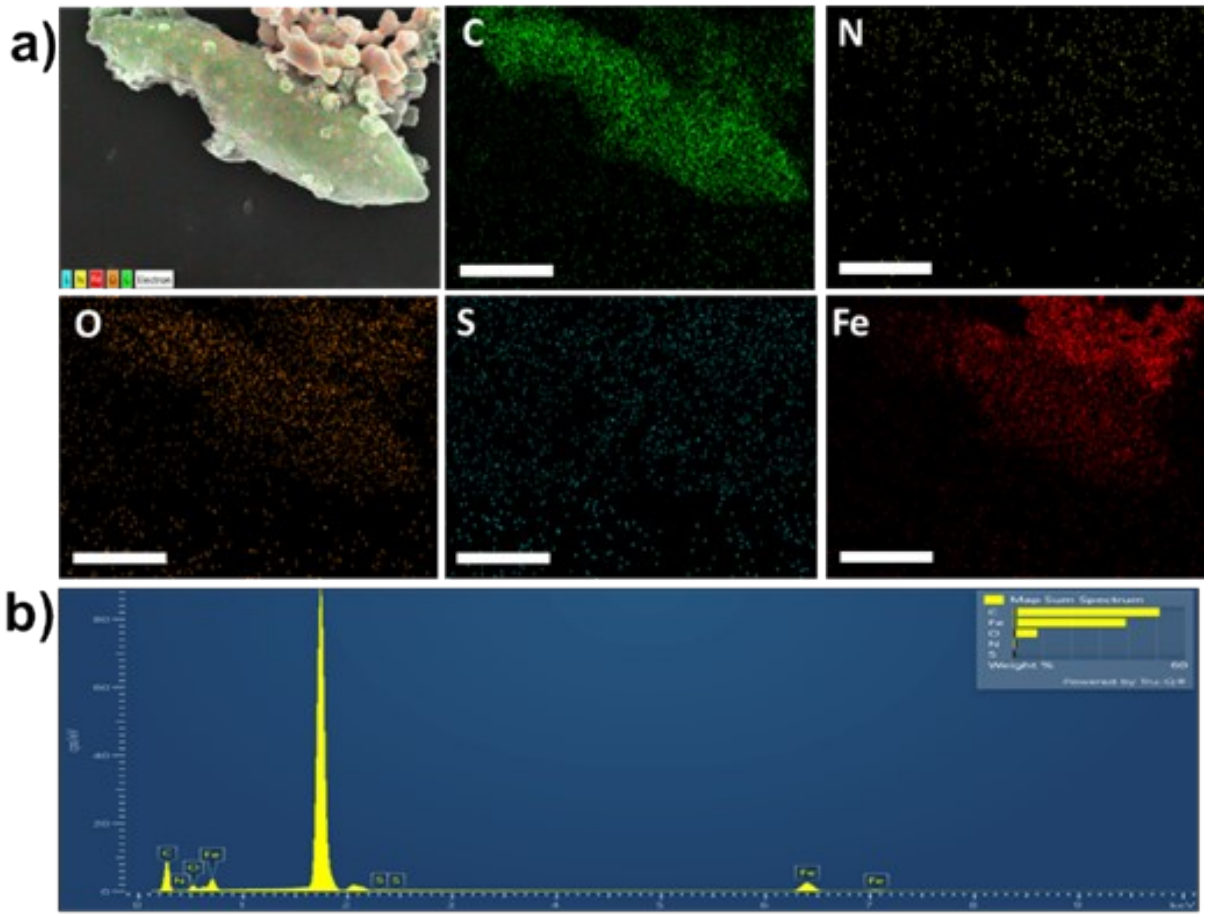

Fig S15. a, b) SEM elemental mapping of the post-catalytic thermal decomposed Fe-MOF after catalytic sample (scale bar 2.5µm).

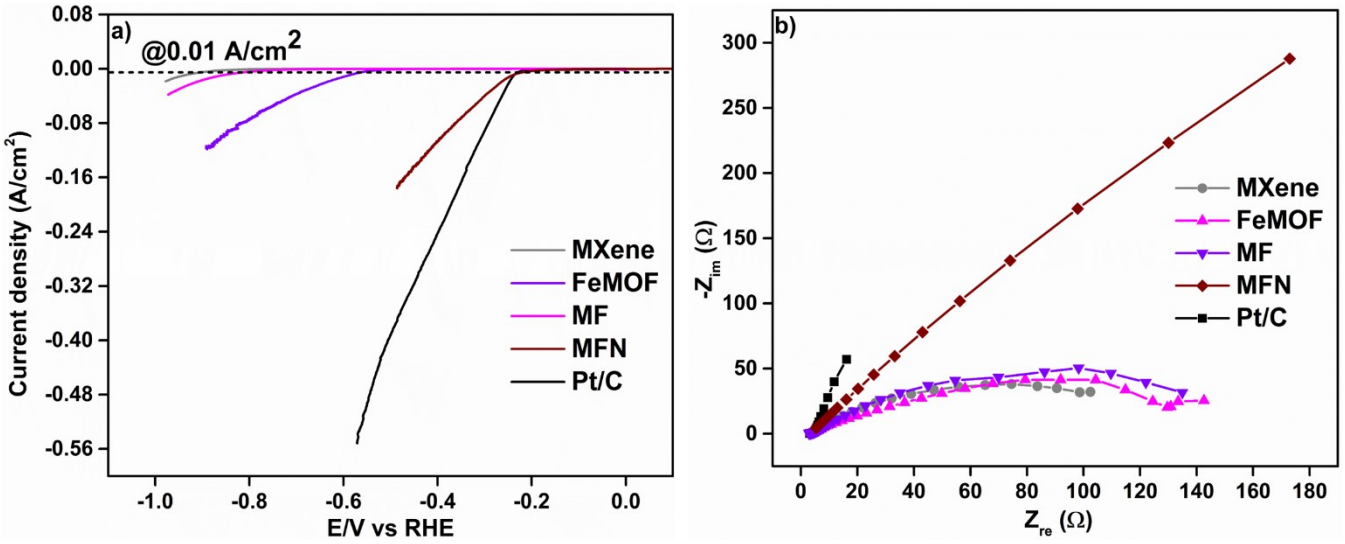

Fig S16. a) LSV polarization of synthesized materials with graphite rod as counter electrode

b) EIS analysis of the synthesized materials with graphite rod as counter electrode.

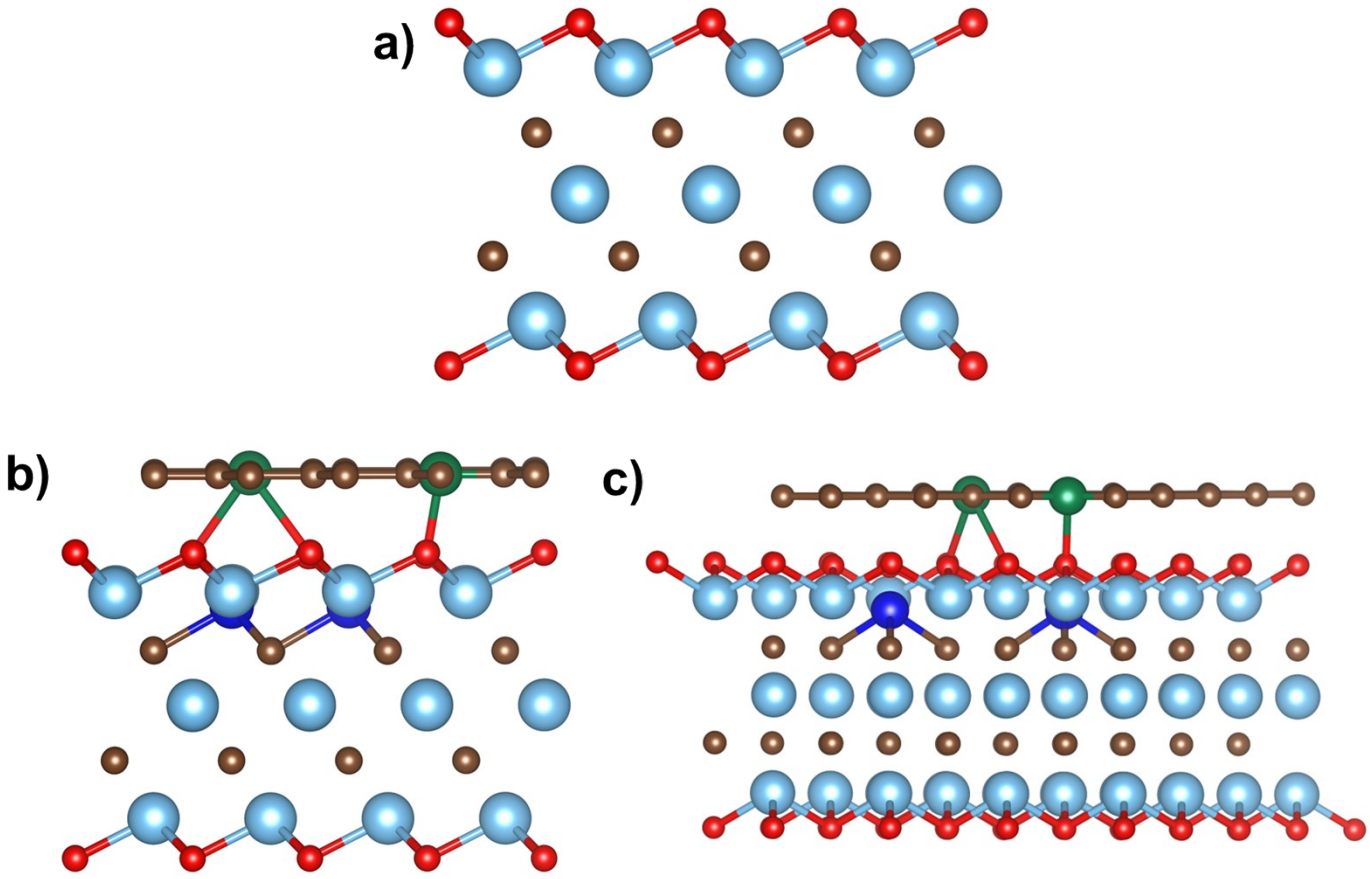

Fig S17. a) Side view of optimized slab model of MXene ($Ti_3C_2O_2$) **b, c)** Two different side view of optimized slab models of MFN (MXene ($Ti_3C_2O_2$) with Ni SACs and oxide bonded pyrolyzed Fe-MOF) (Atoms in blue, brown, red, green, dark blue represent Ti, C, O, Fe, Ni)

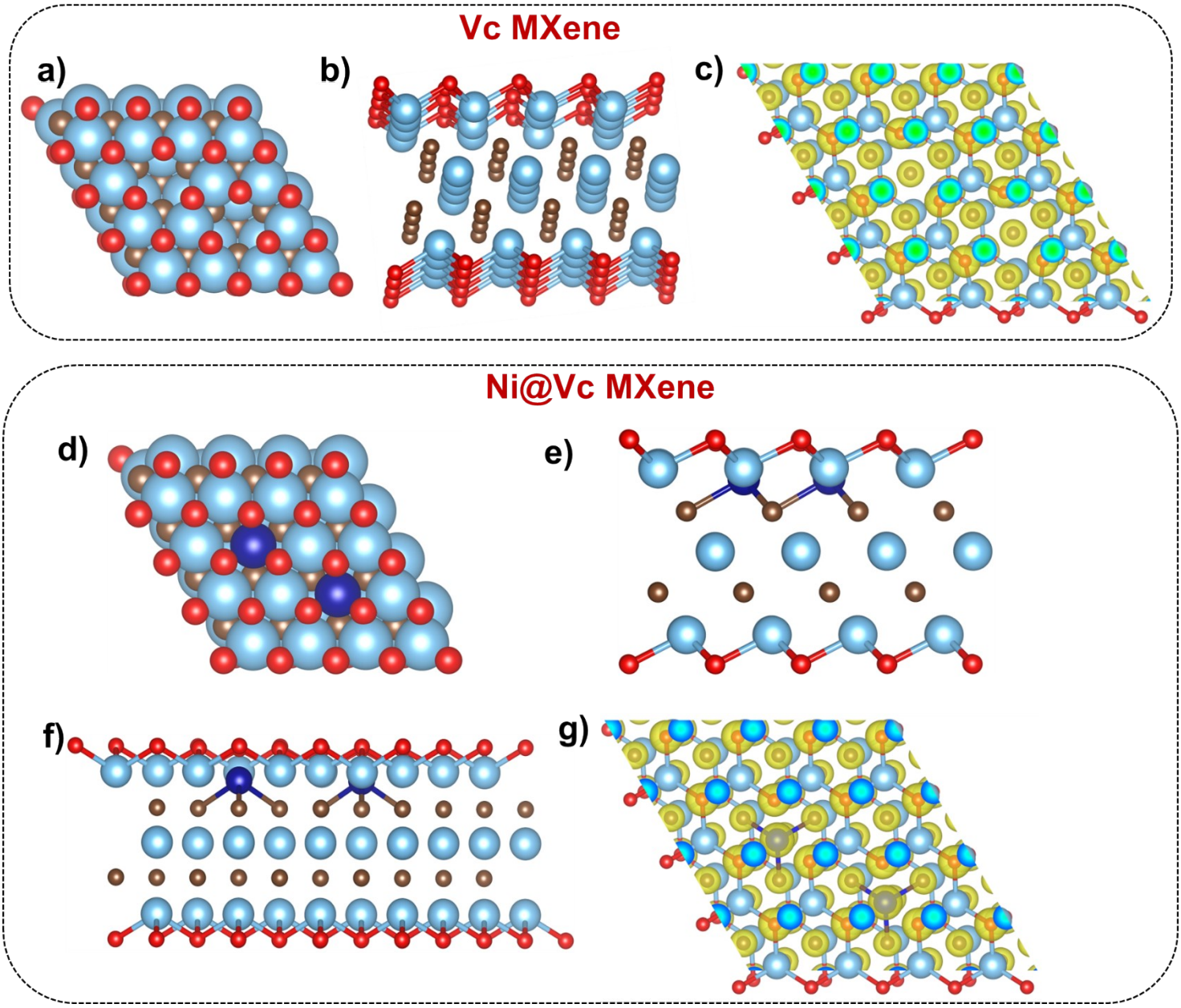

Fig S18. a) Top view of optimized slab models of Vc MXene **b)** Side view of optimized slab models of Vc MXene **c)** Charge density distribution of Vc MXene slab model d) Top view of optimized slab models of Ni@Vc MXene **e, f)** Two different side view of optimized slab models of Ni@Vc MXene **g)** Charge density distribution of Ni@Vc MXene slab model

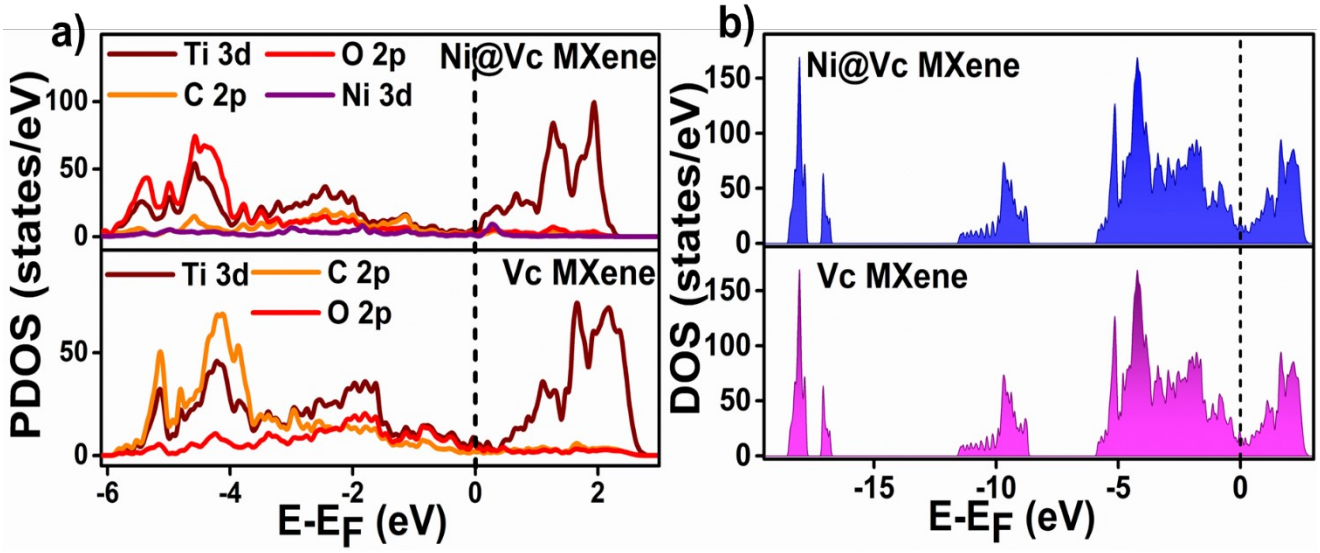

Fig S19. a) Calculated projected density of states (PDOS) of Vc MXene and Ni@Vc MXene with aligned fermi level **b)** Calculated total density of states (TDOS) of Vc MXene and Ni@Vc MXene with aligned fermi level

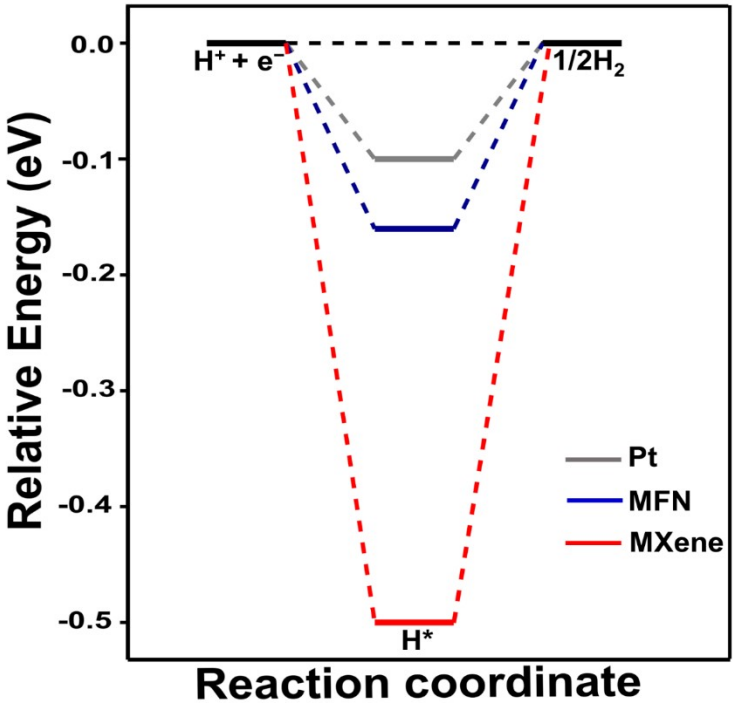

Fig S20. Calculated free energy profiles of HER for Pt, MFN and MXene at the equilibrium potential

References

[1] Dang, Y., Han, P., Li, Y., Zhang, Y. and Zhou, Y., 2020. Low-crystalline mixed Fe-Co-MOFs for efficient oxygen evolution electrocatalysis. *Journal of Materials Science*, *55*, pp.13951-13963.

[2] You, Y., Li, F., Ai, Y., Wei, F., Cui, J., Fu, J., Zheng, M. and Liu, S., 2021. Diblock copolymers directing construction of hierarchically porous metal-organic frameworks for enhanced-performance supercapacitors. *Nanotechnology*, *32*(16), p.165601.

[3] Arshad, F., Tahir, A., ul Haq, T., Duran, H., Hussain, I. and Sher, F., 2022. Fabrication of NiCu interconnected porous nanostructures for highly selective methanol oxidation coupled with hydrogen evolution reaction. international journal of hydrogen energy, 47(85), pp.36118-36128.

[4] Nivetha, R., Gothandapani, K., Raghavan, V., Jacob, G., Sellappan, R., Bhardwaj, P., Pitchaimuthu, S., Kannan, A.N.M., Jeong, S.K. and Grace, A.N., 2020. Highly porous MIL-100 (Fe) for the hydrogen evolution reaction (HER) in acidic and basic media. *ACS omega*, *5*(30), pp.18941-18949.